Elastic Energy of Curvature-Driven Bump Formation on Red Blood Cell Membrane

Richard E. Waugh
Department of Biophysics, School of Medicine and Dentistry, University of Rochester, Rochester, New York 14642 USA

ABSTRACT Model calculations were performed to explore quantitative aspects of the discocyte-echinocyte shape transformation in red blood cells. The shape transformation was assumed to be driven by changes in the preferred curvature of the membrane bilayer and opposed by the elastic shear rigidity of the membrane skeleton. The energy required for echinocyte bump formation was calculated for a range of bump shapes for different preferred curvatures. Energy minima corresponding to nonzero bump heights were found when the stress-free area difference between the membrane leaflets or the spontaneous curvature of the membrane became sufficiently large, but the calculations predict that the membrane can tolerate significant differences in the resting areas of the inner and outer leaflets or significant spontaneous curvature without visible changes in shape. Thus, if the cell is near the threshold for bump formation, the calculations predict that small changes in membrane properties would produce large changes in cellular geometry. These results provide a rational framework for interpreting observations of shape transformations in red cells and for understanding the mechanism by which small changes in membrane elastic properties might lead to significant changes in geometry.

INTRODUCTION

The bilayer couple hypothesis was developed to provide a simple explanation of shape transformations in red blood cells (Sheetz and Singer, 1974). Shortly after its original presentation, mechanical models that formulated the essential physical mechanisms for curvature elasticity and chemically induced bending moments were introduced (Evans, 1974; Evans and Skalak, 1979). However, the actual application of this formulism to shape transformations has never been presented. Some analyses of bump formation have been presented. One of these focused on the geometric aspects of the transformation and did not address issues related to the energetics or mechanics of bump formation (Ferrell et al., 1985). Another presented a more detailed analysis based on a model of the membrane skeleton as an ionic gel (Stokke et al., 1986a). The ionic gel model was used to estimate the magnitude of contractile stresses in the membrane skeleton that would be required to produce shape transformations. Although the model could have been used to assess shape transformations driven by the "bilayer couple," such calculations were not presented. In the present work, we adopt a somewhat simpler approach to evaluate the energetics of shape transformations driven by changes in the preferred curvature of the bilayer and opposed by the shear elasticity of the membrane skeleton.

The motivation for these calculations came from recent studies of combined effects of urea and lysophosphatidylcholine (LPC) on red cell shape (Khodadad et al., 1996). It was observed that at low concentrations of LPC, red cells generally retained their biconcave shape, but when cells suspended in these same concentrations of LPC were subjected to mild treatment with urea, most of the cells were transformed into echinocytes. The goal of the present analysis is to provide an analytical framework with which to assess different hypotheses for the mechanisms leading to the shape transformations that were observed. Treatment with LPC might drive shape transformations by either or both of two mechanisms: either by changing the naturally preferred curvature of the surface (because of the relatively large headgroup compared to its acyl chain region) or by changing the area of one of the bilayer leaflets relative to the other (because it intercalates preferentially into the outer leaflet of the membrane) (Mohandas et al., 1978). Mild treatment with urea, on the other hand, is not known to produce shape transformations in red cells, but its chaotropic activity is known to produce changes in the structure and organization of the membrane skeleton, the structure that provides the membrane with surface shear elasticity. Therefore, the questions to be addressed in the analysis are:

1. How large a difference in the areas of the two leaflets or how large a spontaneous curvature would be required to drive the formation of an echinocyte bump?
2. What is the relative importance of these two mechanisms in driving the shape transformation?
3. How much of a change in membrane shear elasticity would be required for bumps to form at concentrations of LPC at which bumps do not form in the normal cell?

THE MODEL

We consider three elastic energy storage mechanisms of the membrane: shear elasticity, local bending stiffness (curvature elasticity), and nonlocal bending stiffness (bilayer couple). These energies (F_μ, F_{kc}, and F_{kr}, respectively) are

Received for publication 10 April 1995 and in final form 22 November 1995.

Address reprint requests to Dr. Richard E. Waugh, Department of Biophysics, University of Rochester School of Medicine and Dentistry, 601 Elmwood Ave., Rochester, NY 14642. Tel.: 716-275-3768; Fax: 716-275-6007; E-mail: rewaug@rbb1.biophysics.rochester.edu.

0006-3495/96/02/1027/09 $2.00

given by the following expressions (Evans and Skalak, 1979):

$$F_\mu = \mu \int \beta dA, \tag{1}$$

where μ is the membrane shear modulus, β is a measure of the shear deformation of the surface, and A is the surface area;

$$F_{kc} = \frac{k_c}{2} \int (c_m + c_\varphi - c_o)^2 dA, \tag{2}$$

where k_c is the (local) membrane bending stiffness, c_m and c_φ are the principal curvatures of an axisymmetric surface, and the quantity c_o represents the so-called spontaneous curvature of the surface (Helfrich, 1973); and

$$F_{kr} = \frac{k_r}{2h^2 A}(\Delta A - \Delta A_o)^2, \tag{3}$$

where k_r is the nonlocal membrane bending stiffness, h is the separation distance between the neutral surfaces of the two leaflets of the bilayer, ΔA is the difference in the areas of the two leaflets of the bilayer, and ΔA_o is the area difference between the leaflets when both leaflets are stress-free (Božič et al., 1992). The leaflet area difference is related to the integral of the membrane curvature over the entire membrane surface:

$$\Delta A = h \int (c_m + c_\varphi) dA. \tag{4}$$

The parameter β in the first equation is a function of the surface extension ratio, λ, which is the ratio of the length of a material element in the deformed surface to its length in its natural, undeformed state (Evans and Skalak, 1979):

$$\beta = \frac{1}{2}(\lambda^2 + \lambda^{-2} - 2). \tag{5}$$

For the sake of simplicity, we treat the surface as two-dimensionally incompressible, that is, the area of each surface element is assumed to remain fixed, as does the area of the entire membrane. (Recent evidence suggests that this is an oversimplification of the real membrane behavior (Mohandas and Evans, 1994; Discher et al., 1994), but the essential characteristics of the shear elastic energy are captured in Eqs. 1 and 5.) The extension ratio λ depends on the surface deformation. For an axisymmetric deformation of an incompressible surface, it is equal to the ratio of the radial position of the material point in the undeformed state to its radial position in the deformed state (see Fig. 1) (Evans and Skalak, 1979). The value of λ at any position in the deformed surface can be found by equating areas in the deformed and undeformed states. If the initial state is taken as a flat disk, then the extension ratio can be calculated as

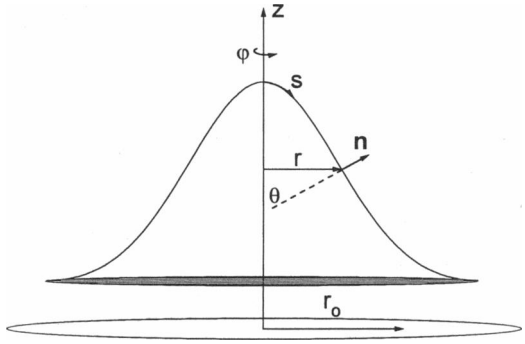

FIGURE 1 Schematic of a bump showing cylindrical coordinates r, z, and ϕ, surface coordinate s, and the angle θ between the surface normal and the axis of symmetry. Note that the location of the material point at r_o in the undeformed disk moves to the radial position r in the deformed surface.

$$\lambda^2 = \frac{r_o^2}{r^2} = \frac{1}{r^2}\int_0^r 2r' ds, \tag{6}$$

where the integral is over the distance along the surface s and is equal to the area of the deformed surface up to the radial position r (divided by π). The principal curvatures of the surface are given in terms of the surface coordinates as

$$c_m = \frac{d\theta}{d_s} \quad \text{and} \quad c_\varphi = \frac{\sin\theta}{r}, \tag{7}$$

where θ is the angle between the surface normal and the axis of symmetry.

It is important to recognize the distinction between the spontaneous curvature c_o and the equilibrium area difference between the two bilayer leaflets ΔA_o. Both arise from asymmetries in the membrane leaflets. The spontaneous curvature results from differences in the packing of the acyl chains and the size of the polar headgroups. For example, lyso-lipids tend to produce an outward curvature to the leaflets. However, if the composition of the leaflets is symmetric, the opposing tendencies of the leaflets will be in balance and there will be no net spontaneous curvature for the bilayer. On the other hand, if one leaflet contains more lysolipid than the other, then there will be a net tendency for the bilayer to curve outward in the direction toward the leaflet with the greater curvature preference. In contrast, the area difference ΔA_o arises primarily from a difference in the number or size of molecules in the two leaflets. Thus, when the leaflets are stress-free, one leaflet might have a larger area than the other, and the contour of the membrane would tend to curve outward in the direction of the leaflet with the greater area. As shown in Eq. 4, ΔA depends on the integral of the membrane curvature over the entire membrane capsule, and negative curvatures in one region may compensate positive curvatures in another region. The term "nonlocal" bending stiffness emphasizes the dependence of this energy on the net curvature over the entire membrane.

It is easily seen that it will not always be possible to have all three energy storage mechanisms at a minimum simultaneously. For example, if the composition of the membrane is such that the spontaneous curvature of the surface is zero, but there is an area difference between the leaflets, then the membrane will tend to curve. This tendency will be opposed by the local curvature elasticity of the membrane (Eq. 2), and (if the membrane has shear rigidity) by the membrane shear elasticity (Eq. 1). The shape that the surface assumes will correspond to a minimum for the sum of all three energy storage mechanisms (subject to the constraints of fixed surface area and volume), but the net elastic energy of the surface will generally not be zero.

This reasoning forms the basis for the following model calculations. We assume that the natural geometry of the surface for shear deformation is that of a flat disk. (Of course, the actual geometry is a biconcave disk, but because we are dealing with one of many bumps on the surface such that the area from which the bump comes is small, then the approximation of the resting geometry as a flat disk is reasonable.) The spontaneous curvature and natural area difference between the leaflets can be set arbitrarily. We then calculate the total energy of the membrane for different bump geometries and look for the bump size and shape that give us a minimum for the total energy. The area of the bump is constrained to be constant.

CALCULATIONS

An algebraic expression was developed to approximate the geometry of projections observed microscopically on the surfaces of echinocytes. The contour was assumed to be axisymmetric and so could be defined by an expression for the height z as a function of the radial position r. The radius at the base of the projection was taken to be a. The requirements for the function were that the height of the contour must be positive at all points, except at the boundary, where the height should be zero. The slope of the contour should be nonzero at all points except at the tip of the projection and at the boundary. Furthermore, the formulation should contain a sufficient number of free parameters so that the constraint of constant area could be satisfied, and that the height and shape of the contour could be varied within this constraint. The class of shapes for which the energies were calculated was given by the following expression:

$$z = L_o\left[\left(\frac{r}{a}\right)^8 + b\left(\frac{r}{a}\right)^6 - 2(1+b)\left(\frac{r}{a}\right)^4 + b\left(\frac{r}{a}\right)^2 + 1\right]\cdot e^{-4C_{ex}\left(\frac{r}{a}\right)^2}. \tag{8}$$

Note that this formulation satisfies the criteria outlined above. The parameter a was determined by the constraint of constant area. The bump height L_o, the coefficient C_{ex} in the exponential term, and the coefficient b in the polynomial could be varied to adjust the bump shape. In practice, the energy of the bump was found to be relatively insensitive to the value of b, and this parameter was arbitrarily set to a constant value of -2. The range of possible shapes considered in the calculations encompassed bump heights from 0.1 to 3.1 μm and values for the parameter C_{ex} ranged from 1.0 to 30.0. The shapes corresponding to this range are illustrated in Fig. 2.

The calculation of the energy requires determination of the principal curvatures and the surface extension ratio over the particular contour. The curvatures can be obtained from knowing the normal angle θ as a function of the radial coordinate r. For axisymmetric surfaces, the normal angle θ, the surface coordinate s, the radial coordinate r, and the axial coordinate z obey the following relationships:

$$\frac{dz}{dr} = -\tan\theta \tag{9}$$

$$\frac{dr}{ds} = \cos\theta \;\Rightarrow\; ds = \left[\left(\frac{dz}{dr}\right)^2 + 1\right]^{1/2} dr. \tag{10}$$

For the contour given by Eq. 8, these relationships and the surface curvatures defined in Eq. 7 are given by

$$\frac{dz}{dr} = -\tan\theta = L_o P_t e^{-cr^2/a^2} \tag{11}$$

$$c_m = -\frac{L_o P_s}{P_c^3} e^{-cr^2/a^2} \tag{12}$$

$$c_\varphi = -\frac{L_o P_t}{r P_c} e^{-cr^2/a^2}, \tag{13}$$

where the parameters P are defined:

$$P_c = \frac{1}{\cos\theta} = [(L_o P_t e^{-cr^2/a^2})^2 + 1]^{1/2} \tag{14}$$

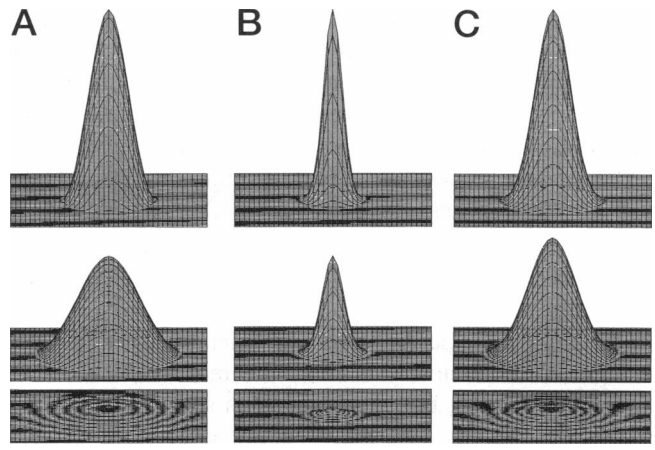

FIGURE 2 The range of possible shapes considered in the analysis is shown for bump heights of L_o = 0.1, 1.6, and 3.1 μm. (*A*) Shapes corresponding to a gaussian coefficient C_{ex} = 1.0; (*B*) shapes for C_{ex} = 30. Usually the shape corresponding to the minimum energy had a value of C_{ex} = 2.5. Three of these shapes are shown in *C*.

$$P_t = \frac{1}{a}\left\{ -2c\left(\frac{r}{a}\right)^9 + (8 - 2cb)\left(\frac{r}{a}\right)^7 + \left(6b + 4cb + 4c\right)\left(\frac{r}{a}\right)^5 - (8b + 8 + 2cb)\left(\frac{r}{a}\right)^3 + 2(b - c)\left(\frac{r}{a}\right)\right. \quad (15)$$

$$P_s = \frac{1}{a^2}\left\{4c^2\left(\frac{r}{a}\right)^{10} + (4c^2b - 34c)\left(\frac{r}{a}\right)^8 + (56 - 26cb - 8c^2(b + 1))\left(\frac{r}{a}\right)^6 - (30b + 4c^2b + 36c(b + 1))\left(\frac{r}{a}\right)^4 + (4c^2 - 10cb - 24(b + 1))\left(\frac{r}{a}\right) + 2(b - c)\right\} \quad (16)$$

(In the equations above we substituted the symbol c for C_{ex} to simplify the notation.) The surface extension ratio λ was calculated according to Eq. 6, where $ds = P_c dr$.

To begin the calculations, the parameter b was set to -2, and values for the projection height L_o and the exponential coefficient C_{ex} were chosen. A trial value for the intercept a was chosen, and the contour was integrated numerically to determine its area. The parameter a was adjusted to make the area of the contour equal to the specified fraction of the total cell area. For most calculations, it was assumed that there were 20 spikes on the cell surface, each with an area of 7.0 μm^2. (The results of the energy calculations did not depend strongly on the number of bumps chosen.) Once the value of a was determined that gave the proper value for the bump area, the contour was integrated again to determine the free energy of the bump corresponding to each of the elastic energies, F_μ, F_{kc}, and F_{kr}, as well as the total energy. The calculations were performed for a range of values of L_o and C_{ex} to construct an energy surface showing the energy as a function of L_o and C_{ex} for each specified set of values for the spontaneous curvature c_o, the leaflet area difference ΔA_o, and the membrane shear modulus μ. The values of L_o and C_{ex} corresponding to the minimum energy were obtained by inspection.

RESULTS

Calculations were performed for parameter values that were thought to most closely emulate the real membrane. For normal membrane, the value of μ was set at 0.005 mN/m (Waugh and Evans, 1979), the membrane bending stiffness was set at 2.0×10^{-19} J (Evans, 1983; Waugh and Bauserman, 1995), and the nonlocal bending modulus was set to 4.0×10^{-19} J (Waugh and Bauserman, 1995). The addition of LPC to the membrane was expected to affect both the spontaneous curvature of the surface and the area difference between the leaflets. The spontaneous radius of curvature of the membrane for a 1% mol concentration of LPC was estimated to be ~ 1.0 μm (corresponding to a total curvature of 2.0×10^6 m^{-1}), and this curvature was assumed to increase or decrease in proportion to the LPC content (see Appendix). Thus, for the first series of calculations, a fractional difference in the leaflet areas of 0.01 was assumed to correspond to a spontaneous curvature of 2×10^6 m^{-1}, an area difference of 0.02 was assumed to correspond to a spontaneous curvature of 4×10^6 m^{-1}, and so on.

The results of this first series of calculations are shown in Fig. 3. Note that for values of the fractional area difference less than or equal to 0.010, and spontaneous curvature less than or equal to 2.0×10^6 m^{-1}, the energy minimum occurred at a bump height of zero. For values of $\Delta A_o/A$ of 0.02 or greater, the predicted bump became progressively taller and (because area was constrained to remain constant) the base became narrower. A second series of calculations was performed to examine the transition region more carefully (Fig. 4). At $\Delta A_o/A = 0.014$, the energy minimum remained at $L_o = 0.0$, that is, no bump was predicted to form. At a fractional area difference of 0.015, a metastable minimum appeared at a bump height of approximately 0.85 μm, and at a $\Delta A_o/A$ value of 0.016, a stable minimum appeared at a bump height of 1.0 μm. Thus, over a very small range of area difference (and spontaneous curvature) values, an abrupt change in surface geometry was predicted.

When a minimum of the energy was found at nonzero bump height, only one minimum was ever found within the range of parameters that were tested. Furthermore, the energy associated with the formation of a bump ($\sim 10^{-17}$ J) is much greater than kT ($\sim 4 \times 10^{-21}$ J). Thus, the predicted bump height appeared to be unique and stable, except near the transition region, where the energies for zero or finite bump heights were comparable. The finding of two physically realizable minima in the energy near the transition point is consistent with experimental observations that discocytes and echinocytes are often found in the same preparation of cells under conditions that are just sufficient to form echinocytes.

The relative importance of the spontaneous curvature and the fractional area difference were evaluated by setting each of these parameters to zero in turn. When the spontaneous curvature was set to zero, there was surprisingly little effect on the analytical predictions (see Fig. 5). The transition point increased from a value of 0.015 for $\Delta A_o/A$ (for $c_o = 3 \times 10^6$ m^{-1}) to a value of approximately 0.018 (for $c_o = 0.0$). This is also evident in Fig. 6, which shows the bump height corresponding to the lowest energy as a function of $\Delta A_o/A$. In this figure the spontaneous curvature was assumed to increase in proportion to $\Delta A_o/A$, and the different curves correspond to different ratios of $c_o/(\Delta A_o/A)$ ranging from 0.0 to 3.0×10^8 m^{-1}. The behavior was similar regardless of the ratio, but the point at which the transition occurred decreased slightly as the ratio increased. In contrast, when $\Delta A_o/A$ was set to zero, the energy minimum remained at a bump height of zero until the spontaneous

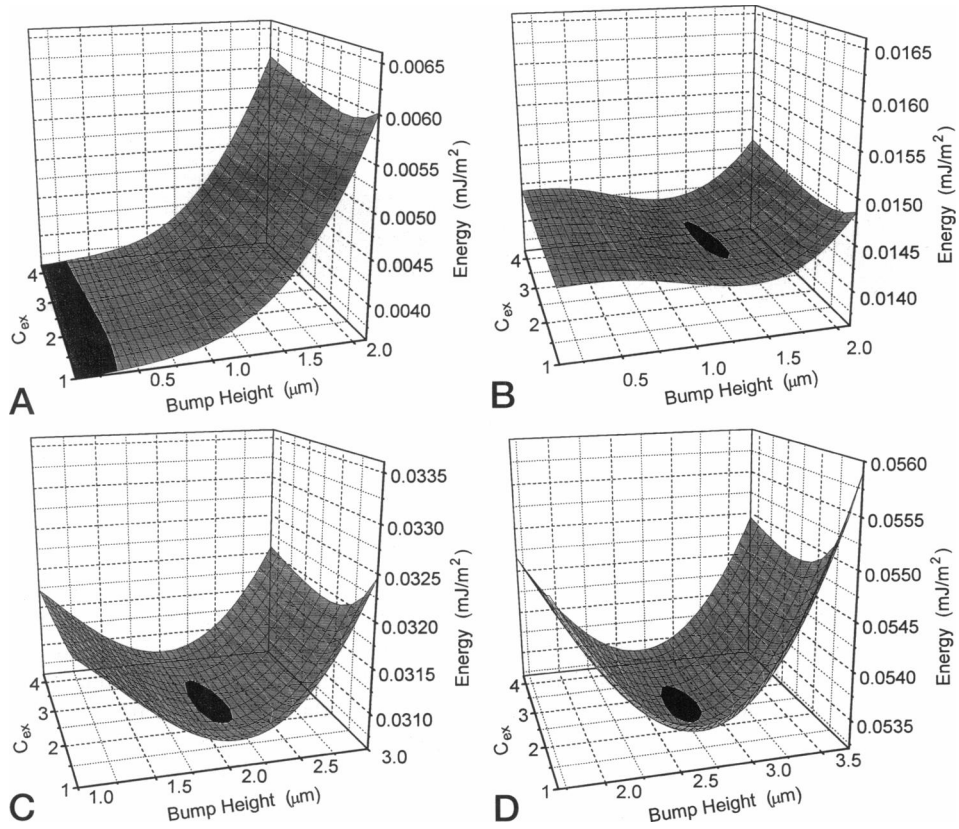

FIGURE 3 Energy surfaces for different values of $\Delta A_o/A$ and c_o. The energy is shown as a function of the exponential coefficient C_{ex} and the bump height. The ratio of the spontaneous curvature c_o to the fractional area difference $\Delta A_o/A$ was kept constant at a value of 2.0×10^8 m^{-1}, and $\mu = 5$ μN/m. Darkly shaded areas indicate the location of the minimum energy. The fractional area difference ($\Delta A_o/A$) and the corresponding bump height L_o were: (*A*) $\Delta A_o/A = 0.01$, $L_o = 0.0$ μm; (*B*) $\Delta A_o/A = 0.02$, $L_o = 1.3$ μm; (*C*) $\Delta A_o/A = 0.03$, $L_o = 2.1$ μm; (*D*) $\Delta A_o/A = 0.04$, $L_o = 2.75$ μm. The exponential coefficient for all minima was approximately 2.5. Note that the scales of the axes are the same for all figures, but the ranges may be different.

curvature reached values in excess of 1.5×10^7 m^{-1} (see Fig. 5 *B*), a value five times larger than the spontaneous curvature corresponding to the transition point shown in Fig. 4. In other words, the spontaneous curvature required to produce a shape transformation is five times larger than the spontaneous curvature expected to result from a concentration of LPC needed to produce a leaflet area difference sufficient to produce the same transformation (see Appendix). Thus, the difference between the areas of the two leaflets appears to be five times more potent a driving force

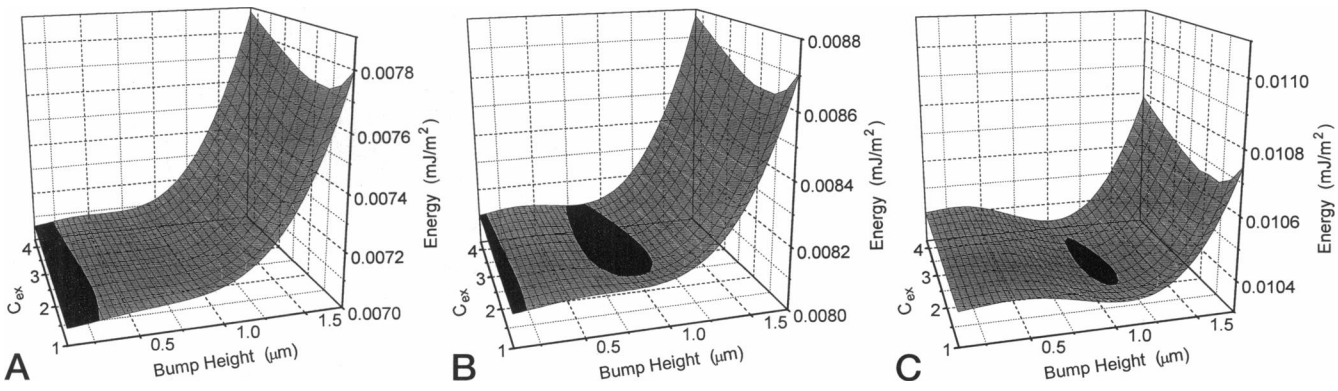

FIGURE 4 The energy is shown as a function of the exponential coefficient C_{ex} and the bump height for values of $\Delta A_o/A$ and c_o near the transition point at which the bump height corresponding to the minimum energy changes abruptly from zero to a finite height. The ratio of c_o to $\Delta A_o/A_o$ was fixed at a value of 2.0×10^8 m^{-1}. At $\Delta A_o/A = 0.014$, the bump height for the minimum energy was zero (*A*). For $\Delta A_o/A = 0.015$, a metastable minimum appears at a bump height of 0.85 μm, and for $\Delta A_o/A = 0.016$, the minimum energy corresponds to a bump height of 1.0 μm ($\mu = 5$ μN/m). Note that the scales of the axes are the same for all of these figures, but the ranges may be different. Also note that the energy scale is different from that of Fig. 3.

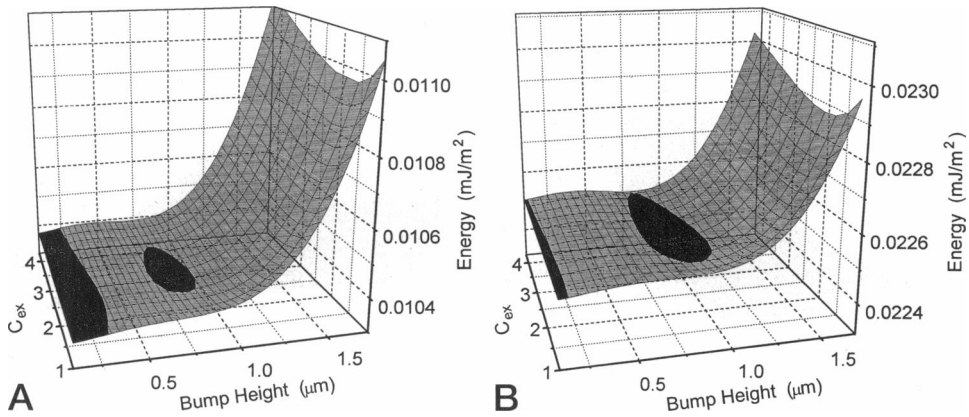

FIGURE 5 This figure illustrates the different effects of $\Delta A_o/A$ and c_o on the transition from zero to finite bump height. When c_o was set to zero, the transition occurred for a value of $\Delta A_o/A$ of approximately 0.018, only slightly different from the transition point when the value of c_o was a fixed proportion of $\Delta A_o/A$ (compare *A* with Fig. 4 *B*). When $\Delta A_o/A$ was set to zero (*B*), the value of c_o required to produce the transition was 15×10^6 m^{-1}, a value five times larger than the value of c_o corresponding to the transition shown in Fig. 4 (μ = 5 μN/m).

for shape change than spontaneous curvature. This result also reveals that the conclusions reached from the calculations do not depend critically on the constant of proportion relating spontaneous curvature to area difference, as the predicted transition hardly changed whether the ratio was zero or 3×10^8 m^{-1}.

The results of the calculations also were insensitive to the number of spikes on the surface over the range of 8 to 24. The energy minimum for 8 or 24 spikes occurred at a value for $\Delta A_o/A$ of approximately 0.015 (not shown).

Finally, to evaluate the possible mechanism by which urea might cause echinocytes to form, we tested the effects of changing the membrane shear modulus. Measurements of the shear modulus in 1.5 M urea revealed a reduction in the modulus of approximately 20% (Khodadad et al., 1996). When the modulus in the calculations was reduced from 0.005 to 0.004 mN/m, projections were predicted to form at $\Delta A_o/A$ = 0.014, a value at which bumps were not predicted to form when the modulus was 0.005 mN/m (see Figs. 4 *A* and 7). Thus, the calculations indicate that if the cell is very near the threshold at which projections will form, a very small reduction in the shear modulus can result in dramatic changes in cellular geometry.

DISCUSSION

This analysis provides important insights for understanding the mechanisms underlying red cell shape transformations

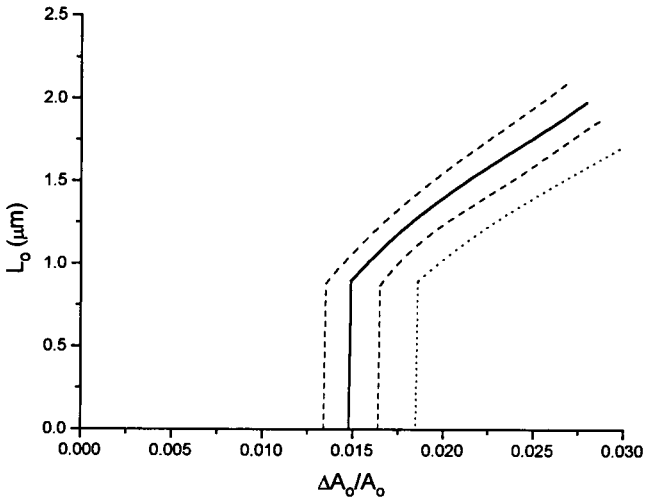

FIGURE 6 The height of the membrane projection L_o at which the minimum energy occurs as a function of the initial area difference between the leaflets, $\Delta A_o/A$. The four curves correspond to different values for the ratio of the spontaneous curvature (c_o) to the fractional leaflet area difference, $\Delta A_o/A$. Moving from the dotted curve at the right to the dashed curve at the left, the ratios were 0.0, 1.0×10^8 m^{-1}, 2.0×10^8 m^{-1}, and 3.0×10^8 m^{-1}, respectively. Note the abrupt nature of the transition from zero to finite bump height.

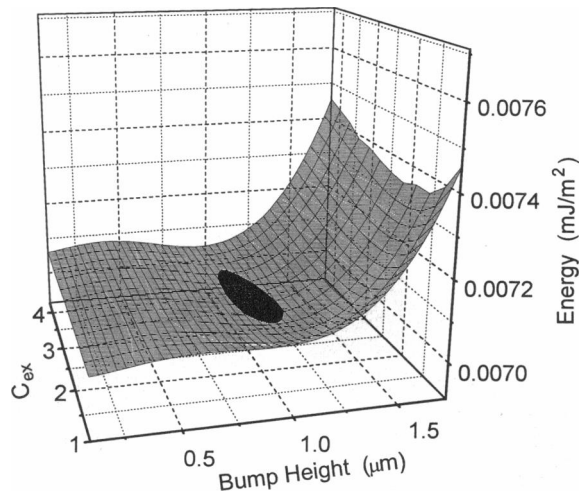

FIGURE 7 This figure illustrates the effect of changing shear modulus on the location of the energy minimum when the membrane is near the transition region. The values for $\Delta A_o/A$ and c_o in this figure were the same as those used to produce Fig. 4 *A*, but the membrane shear modulus was reduced from 5 μN/m to 4 μN/m. Note that in Fig. 4 *A* the minimum energy corresponded to zero bump height, but when the modulus is lower, a stable bump with height 1.15 μm is predicted.

such as those described in a companion report (Khodadad et al., 1996). The analysis indicates that red cells can support significant differences in the stress-free areas of the leaflets of the bilayer without visible alterations in surface geometry. It also indicates that the onset of echinocyte formation is highly nonlinear, and that the transition from disk to echinocyte occurs over a very narrow range of the parameter space. Thus, if a cell challenged by shape-transforming agents is very near the transition point, small changes in membrane elasticity can produce dramatic changes in cellular geometry.

The calculations predict that echinocytes should begin to form when the area difference between leaflets is approximately 1.5%. This prediction is in good agreement with the observations of Lange and Slayton (1993) and Ferrell and colleagues (1985), who measured the amount of LPC (or other lipid) needed to be incorporated into the membrane to produce echinocytes. Ferrell and colleagues estimated that lipid incorporation sufficient to produce a difference in the leaflet areas of 1.5% was needed to produce (stage 2) echinocytes. Lange and Slayton estimated that a mole fraction of LPC in the outer leaflet of 2% (compared to total phospholipid) was the threshold for echinocyte formation. Considering that the area occupied by an LPC molecule is probably less than the area occupied by lecithin, this result is also in excellent agreement with the analytical predictions.

Limitations of the analysis

Although these calculations provide important insights, it should be emphasized that they are based on a simplified, approximate model of the actual cell behavior. The geometry of the bump was limited to a particular class of contours, and so the geometry was not optimized to produce the absolute global energy minimum for all possible contours. Thus, quantitative differences might be observed if different formulations for the bump shape were used. However, the calculated energies were relatively insensitive to changes in the contour parameters b and C_{ex}, indicating that small inaccuracies in the contour shape will not have dramatic effects on the outcome of the analysis. This, plus the fact that the shapes of the model contours closely resemble real projections observed on the surfaces of echinocytes, supports the expectation that the qualitative aspects of the conclusions, namely that the discocyte-echinocyte transition is abrupt and nonlinear, and that the difference between the areas of the bilayer leaflets is a more important driving force for shape transformations than spontaneous curvature, will hold for more exact formulations.

The second limitation of the analysis is that it does not include a constraint on the cell volume. For the questions being addressed in the present work, this is not a serious flaw, because at the onset of bump formation, there is still a large excess of membrane area, and the shape of the cell body can change relatively freely to accommodate the constraint on cell volume. This is evident from the appearance of "reversed curvature" in cells near the transition region as observed in LPC-treated cells (Khodadad et al., 1996). However, if the cell approaches the stage of a spherocechinocyte, clearly the volume constraint will be important as the body of the cell rounds up to a spherical shape. In this case, the pressure difference across the membrane and the resulting stresses in the membrane are likely to become significant contributors to the determination of cell shape. We estimated the point at which the cell volume constraint would become an important factor in the analysis by calculating the volume of the bumps plus an underlying spherical cell body. The size of the sphere was determined by summing the total surface areas of the bases of the bumps, and calculating the volume of a sphere with the same area. (This is roughly equivalent to placing all of the bumps on a sphere such that the average overlap or spacing between bumps is zero.) As long as the volume of the sphere plus the bumps was larger than the cell volume, the volume constraint was not expected to be important, because the sphere could easily take on a more prolate or oblate geometry to "lose" the extra volume. For a surface with 20 bumps, the volume constraint appeared to come into play for bump heights of approximately 1.9 μm, corresponding to the expected bump shape for a fractional stress-free leaflet area difference of approximately 0.03. This should be taken as an approximate upper bound for the applicability of the present approach.

The third feature of cell behavior that is not accounted for in the present analysis is the possibility that cellular properties and the distribution of molecular components may be nonuniform over the cell surface. Recently, evidence was presented that when the membrane is subjected to large deformations, the density of the membrane skeleton becomes nonuniform (Discher et al., 1994). Thus, an obvious extension of the present model would be to include such behavior in calculating the energy due to shear deformation. Although such an approach would be a more exact model of the cellular behavior, it was not included in the present analysis because it would add significant complexity to the calculations and it is not expected to alter the basic conclusions of the analysis. Discher et al. (1994) have shown that the ratio of the modulus for skeletal dilation (K_s) to the skeletal shear modulus (μ) is approximately 2.0. At this ratio, the predicted behavior of the membrane during the formation of surface projections of the size of those considered in the present analysis is not significantly different, whether it is assumed that the membrane skeleton is compressible or not. This conclusion is based on the calculations of Stokke et al. (1986a,b) and is made while recognizing that the value of the elastic shear modulus that is calculated from micropipette aspiration experiments also depends on the ratio of the dilational to the extensional modulus of the membrane skeleton. (Inspection of figure 9 of Stokke et al. (1986a) appears to show markedly different energies for different ratios of K_s/μ, but the reader should recognize that the plotted values of the energy are normalized by the shear

modulus. Inspection of figure 2 of Stokke et al. (1986b) reveals that the value of the modulus determined from measurements of projection length versus aspiration pressure in micropipette aspiration studies will also depend on the value of K_s/μ. Although the normalized energy shown in figure 9 of Stokke et al. (1986a) appears smaller for $K_s/\mu = 1.0$ than for $K_s/\mu = \infty$, the larger value of the modulus determined for $K_s/\mu = 1.0$ from Fig. 2 (Stokke et al., 1986b) compensates for the apparent difference almost exactly (within 3%).) Physically, the reason that this is true is that the shear modulus was determined from measurements of bump formation (using micropipettes), a deformation similar to the one analyzed in the present work. Using the same constitutive model in both cases provides a consistent estimate of the elastic energy associated with the deformations. The value of the shear modulus used in the present calculations was determined from micropipette aspiration measurements assuming that the membrane skeleton was incompressible, the same constitutive model used in the present calculations. Thus, this value of the modulus provides a consistent estimate of the (elastic shear deformation) energy required to form bumps of dimensions used in the present calculations.

A second potential source of nonuniformity of membrane behavior could arise from nonuniform distribution of LPC over the surface, leading to regions of different spontaneous curvature. Although such a possibility cannot be ruled out entirely, the following arguments indicate that it should not be a serious concern. The first point is that the primary driving force for shape transformation is the area difference between the leaflets, not the spontaneous curvature. Thus, large spatial variations in LPC concentration would be needed to have a significant effect on the membrane contour. Second, lateral segregation of LPC would be opposed by the free energy of mixing, which is large compared to the curvature energy (Song and Waugh, 1993). Thus, in the absence of other factors leading to phase separation, curvature by itself is not expected to produce significant lateral gradients in LPC concentration.

CONCLUSIONS

These calculations provide the following answers to the questions posed at the beginning of this paper. For reasonable values of the membrane elastic coefficients, a stress-free area difference between the membrane leaflets of approximately 1.5% is required to produce a transformation from discocyte to echinocyte. The spontaneous curvature required to produce the same transformation corresponds to a significantly higher concentration of LPC in the membrane, leading to the conclusion that it is the area difference that is the primary driving force for shape transformation. An unexpected result of the calculations was the abrupt nature of the transition from smooth surface to bump as the stress-free area difference between the leaflets increased. This feature of the membrane behavior leads to the prediction that if a cell is near this transition point, small changes in the shear rigidity of the membrane can lead to dramatic changes in cellular geometry.

APPENDIX

In this appendix we estimate the spontaneous curvature of the membrane resulting from the presence of LPC in one of the membrane leaflets. The spontaneous curvature was estimated by treating the monolayer as two surfaces, one corresponding to the headgroup region, one corresponding to the acyl chain region. It was assumed that in the natural membrane, the areas of these two layers are equal. It was further assumed that addition of LPC adds half the area per molecule to the acyl chain region as it does to the headgroup region. Thus, making the mole fraction of LPC in the membrane equal to 1% would add 1% to the area of the headgroup region but only 0.5% to the acyl chain region. The difference between the area of the headgroups and the area of the acyl chain region ΔA_{hc} was assumed to be related to the spontaneous curvature c_o by

$$c_o = \frac{\Delta A_{hc}}{h_{hc} A}, \tag{A1}$$

where h_{hc} is the separation distance between the headgroups and the acyl chains. Taking h_{hc} to be 1.25 nm, the spontaneous curvature corresponding to a 1% molar concentration of LPC was calculated to be $4 \times 10^6\ m^{-1}$ for the individual monolayer. If the other leaflet of the bilayer has zero spontaneous curvature, the net spontaneous curvature for the two leaflets would be $2 \times 10^6\ m^{-1}$. For a spherical surface segment, this corresponds to a radius of 1.0 μm. As the concentration of LPC in the leaflet increases, the spontaneous curvature is expected to increase in direct proportion.

The author thanks Dr. Ted Steck for his reading of the manuscript and for pointing out the work of Lange and Slayton.

This work was supported by a grant from the U.S. Public Health Service (HL 31524).

REFERENCES

Božič, B., S. Svetina, B. Žekš, and R. E. Waugh. 1992. Role of lamellar membrane structure in tether formation from bilayer vesicles. *Biophys. J.* 61:963–973.

Discher, D. E., N. Mohandas, and E. A. Evans. 1994. Molecular maps of red cell deformation: hidden elasticity and in situ connectivity. *Science.* 266:1032–1035.

Evans, E. A. 1974. Bending resistance and chemically induced moments in membrane bilayers. *Biophys. J.* 14:923–931.

Evans, E. A. 1983. Bending elastic modulus of red blood cell membrane derived from buckling instability in micropipet aspiration tests. *Biophys. J.* 43:27–30.

Evans, E. A., and R. Skalak. 1979. Mechanics and thermodynamics of biomembranes. *CRC Crit. Rev. Bioeng.* 3:181–418.

Ferrell, J. E., K. J. Lee, and W. H. Huestis. 1985. Membrane bilayer balance and erythrocyte shape: a quantitative assessment. *Biochemistry.* 24:2849–2857.

Helfrich, W. 1973. Elastic properties of lipid bilayers: theory and possible experiments. *Z. Naturforsch.* C28:693.

Khodadad, J. K., R. E. Waugh, J. L. Podolski, R. Josephs, and T. L. Steck. 1996. Remodeling the shape of the skeleton in the intact red cell. *Biophys. J.* 70:In press.

Lange, Y., and J. M. Slayton. 1993. Interaction of cholesterol and lysophosphatidylcholine in determining red cell shape. *J. Lipid Res.* 23: 1121–1127.

Mohandas, N., and E. A. Evans. 1994. Mechanical properties of the red cell membrane in relation to molecular structure and genetic defects. *Annu. Rev. Biophys. Biomol. Struct.* 23:787–818.

Mohandas, N., A. C. Greenquist, and S. B. Shohet. 1978. Bilayer balance and regulation of red cell shape. *J. Supramol. Struct. Cell. Biochem.* 9:453–458.

Sheetz, M. P., and S. J. Singer. 1974. Biological membranes as bilayer couples. A molecular mechanism of drug-erythrocyte interactions. *Proc. Natl. Acad. Sci. USA.* 71:4457–4461.

Song, J. B., and R. E. Waugh. 1993. Bending rigidity of SOPC membranes containing cholesterol. *Biophys. J.* 64:1967–1970.

Stokke, B. T., A. Mikkelsen, and A. Elgsaeter. 1986a. The human erythrocyte membrane skeleton may be an ionic gel. II. Numerical analysis of cell shapes and shape transformations. *Eur. Biophys. J.* 13:219–233.

Stokke, B. T., A. Mikkelsen, and A. Elgsaeter. 1986b. The human erythrocyte membrane skeleton may be an ionic gel. III. Micropipette aspiration of unswollen erythrocytes. *J. Theor. Biol.* 123:205–211.

Waugh, R. E., and R. G. Bauserman. 1995. Physical measurements of bilayer-skeletal separation forces. *Ann. Biomed. Eng.* 23:308–321.

Waugh, R., and E. A. Evans. 1979. Thermoelasticity of red blood cell membrane. *Biophys. J.* 26:115–132.